Synthesis and physical properties of $Ce_2Rh_{3+\delta}Sb_4$ single crystals

Kangqiao Cheng,[1,*] Shuo Zou,[1,*] Huanpeng Bu,[2] Jiawen Zhang,[3] Shijie Song,[3] Hanjie Guo,[2,†] Huiqiu Yuan,[3,‡] and Yongkang Luo[1,§]

[1]*Wuhan National High Magnetic Field Center and School of Physics, Huazhong University of Science and Technology, Wuhan 430074, China*
[2]*Songshan Lake Materials Laboratory, Dongguan, Guangdong 523808, China*
[3]*Center for Correlated Matter and School of Physics, Zhejiang University, Hangzhou 310058, China*

(Received 15 May 2023; accepted 21 July 2023; published 16 August 2023)

Millimeter-sized $Ce_2Rh_{3+\delta}Sb_4$ ($\delta \approx 1/8$) single crystals were synthesized by a Bi-flux method, and their physical properties were studied by a combination of electrical transport, magnetic, and thermodynamic measurements. The resistivity anisotropy $\rho_{a,b}/\rho_c \sim 2$, manifesting a quasi-one-dimensional electronic character. Magnetic susceptibility measurements confirm **ab** as the magnetic easy plane. A long-range antiferromagnetic transition occurs at $T_N = 1.4$ K, while clear short-range ordering can be detected well above T_N. The low ordering temperature is ascribed to the large Ce-Ce distance as well as the geometric frustration. Kondo scale is estimated to be about 2.4 K, comparable to the strength of magnetic exchange. $Ce_2Rh_{3+\delta}Sb_4$, therefore, represents a rare example of a dense Kondo lattice whose Ruderman-Kittel-Kasuya-Yosida exchange and Kondo coupling are both weak but competing.

DOI: 10.1103/PhysRevMaterials.7.084404

I. INTRODUCTION

Heavy-fermion compounds are prototypical strongly correlated systems whose electrons can behave rather unconventionally. Examples of the latter include the ubiquitous strange-metal and/or non-Fermi-liquid behavior observed in the vicinity of quantum critical points (QCPs) characterized by subquadratic temperature-dependent resistivity ($\rho \propto T^n$, where n is substantially less than 2), a divergent electronic specific-heat coefficient (e.g., $C/T \propto -\log T$), etc. [1,2]. QCP refers to a continuous termination of a phase transition that leads to the point at absolute zero separating the quantum-ordered and -disordered states on the phase diagram. Of particular interest are ferromagnetic (FM) QCPs. An earlier judgment stated that FM QCPs are usually avoided in clean systems by the occurrence of a first-order transition [3,4], the intersection of antiferromagnetic (AFM) phases [5–7], or a Kondo cluster glass phase [8,9]. However, the past decade has witnessed the discovery of a handful of counterexamples, $YbNi_4(P_{1-x}As_x)_2$ [10,11] and $CeRh_6Ge_4$ [12], where FM QCP seems realized. Irrespective of the inevitable disorder effect caused by chemical doping in $YbNi_4(P_{1-x}As_x)_2$, the pressure-induced continuous suppression of the order parameter and the emergent strange-metal behavior in the pure ferromagnet $CeRh_6Ge_4$ provide a pristine paradigm of FM QCP [12]. The key common features of these two compounds are (i) they both contain quasi-one-dimensional (Q1D) rare-earth chains, and (ii) their ferromagnetism is of easy-plane anisotropy [12–14]. Theoretically, easy-plane anisotropy projects out an equal-spin pair and thus creates a triplet resonant valence bond (tRVB) state $[(|\uparrow\uparrow\rangle + |\downarrow\downarrow\rangle)/2]$ [12]. Macroscopic entanglement can thus be injected into the ground state, i.e., easy-plane anisotropy in FM systems plays a similar role to that of magnetic frustration in antiferromagnetic systems [15], and this favors unconventional, local quantum criticality where the suppression of the order parameter is also accompanied with a destruction of Kondo screening and a reconstruction of the Fermi surface [16–24]. Moreover, as the tRVB states are already present, spin-triplet superconductivity is possible if they can be condensed. For progress, extensive FM materials with Q1D easy-plane anisotropy are needed both to attest to this idea and further guide its development.

Recently, we reported the growth of a new ternary superconducting rhodium-antimonide $La_2Rh_{3+\delta}Sb_4$ ($T_c \sim 0.8$ K) [25]. Previously, this family of compounds (e.g., $Ce_2Rh_3Sb_4$) were recognized to crystallize in the orthorhombic $Pr_2Ir_3Sb_4$ structure, with the space group *Pnma* (No. 62) [26,27]. By careful *single-crystal* x-ray diffraction (XRD) and scanning transmission electron microscope (STEM) measurements [25], we demonstrated the existence of an additional Rh4 site (that was not identified before) whose occupation rate is $\delta \approx 1/8$. In this compound, the La atoms form Q1D chains along **c** (Ref. [28]), and these chains are isolated by Rh-Sb polyhedra, which motivates us to look further into its sister compound $Ce_2Rh_{3+\delta}Sb_4$. In fact, as early as in 2011, Gil *et al.* already reported the growth of polycrystalline $Ce_2Rh_3Sb_4$ [26]. There the temperature dependence of magnetic susceptibility down to 2 K remains Curie-Weiss-like without showing any trace of magnetic ordering. This implies that the system probably sits in a regime close to a quantum criticality. To better clarify the ground state and the possibility of QCP in

*These authors contributed equally to this work.
†hjguo@sslab.org.cn
‡hqyuan@zju.edu.cn
§mpzslyk@gmail.com

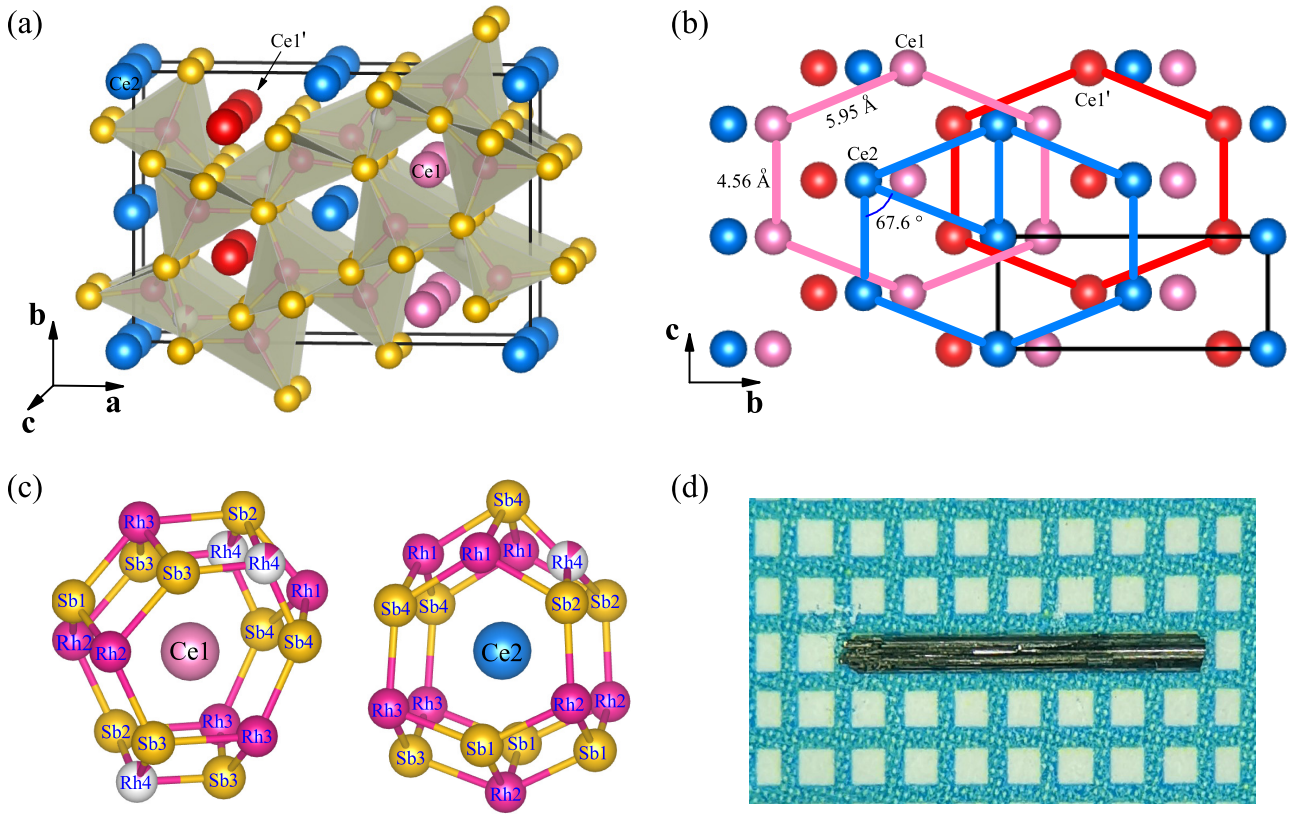

FIG. 1. (a) The crystalline structure of $Ce_2Rh_{3+\delta}Sb_4$. The Ce chains are along the **c**-axis, isolated by the Rh-Sb polyhedra. The partially occupied Rh4 is double-colored. The black rectangle depicts the unit cell. (b) Both Ce1 and Ce2 sublattices form distorted triangular networks within **bc** planes, stacked following the sequence of Ce2-Ce1′-Ce2-Ce1-Ce2 along **a**. (c) Local environments of Ce1 and Ce2. (d) A photograph of $Ce_2Rh_{3+\delta}Sb_4$ single crystal on millimeter-grid paper. The single crystals are needlelike along **c** axis.

this compound, both single-crystal samples and sub-Kelvin measurements are badly needed.

In this paper, we report the synthesis and physical properties of $Ce_2Rh_{3+\delta}Sb_4$ ($\delta \approx 1/8$) single crystals. Our work manifests that $Ce_2Rh_{3+\delta}Sb_4$ is an easy-plane antiferromagnet with Néel temperature $T_N = 1.4$ K. Short-range magnetic correlation can be observed well above T_N. Kondo scale is estimated, $T_K \sim 2.4$ K, comparable to the strength of magnetic exchange. We also discuss the reason for the low ordering temperature, and the possibility of QCP under pressure.

II. EXPERIMENTAL DETAILS

Single-crystalline $Ce_2Rh_{3+\delta}Sb_4$ was grown by a Bi-flux method as described in our earlier work [25]. Ce chunk (Alfa Aesar, 99.9%), Rh powder (Aladdin, 99.95%), Sb granule (Aladdin, 99.9999%), and Bi granule (Aladdin, 99.9999%) were weighed in a molar ratio of 2:3:4:40, and transferred into an alumina crucible that was sealed in an evacuated quartz tube. The latter was heated to 500 °C in 20 h, held for 1 day, and then raised to 1100 °C in 30 h. After keeping at this temperature for 100 h, we slowly cooled it to 500 °C in 2 weeks, and then the Bi-flux was removed by centrifugation. The remaining Bi-flux can be dissolved by a mixture of an equal volume of hydrogen peroxide and acetic acid. The as-grown samples are mostly needlelike with a typical length 3–7 mm along the **c** axis, and about 0.6 × 0.7 mm^2 in cross section [Fig. 1(d)].

The chemical composition of the obtained single crystals was verified by energy-dispersive x-ray spectroscopy (EDS) affiliated with a field emission scanning electron microscope (FEI Model SIRION), which gives the atomic ratio Ce : Rh : Sb = 23.21 : 32.56 : 44.24. Single-crystalline x-ray diffraction (XRD) data were recorded at room temperature on a Rigaku XtaLAB mini II with Mo radiation ($\lambda_{K\alpha} = 0.710\,73$ Å). Electrical resistivity was measured by the standard four-probe method in a Physical Property Measurement System (PPMS-9, Quantum Design), which was also used for the specific-heat measurements. To measure the in-plane resistivity, we employed the focused-ion-beam (FIB) technique to make the microstructured device, as shown in the inset to Fig. 2(a). Magnetization measurements were performed using a Magnetic Property Measurement System (MPMS-VSM, Quantum Design) that is equipped with a ^{3}He refrigerator.

III. RESULTS AND DISCUSSION

The crystalline structure of $Ce_2Rh_{3+\delta}Sb_4$ determined from single-crystal XRD analysis is shown in Fig. 1(a). The obtained cell parameters are $a = 16.1927(11)$ Å, $b = 4.5613(3)$ Å, $c = 10.9917(8)$ Å [28], $\alpha = \beta = \gamma = 90°$, and $Z = 4$. The occupation rate of Rh4 is 0.123(3), close to that in $La_2Rh_{3+\delta}Sb_4$ [25]. Ce atoms form chains along the

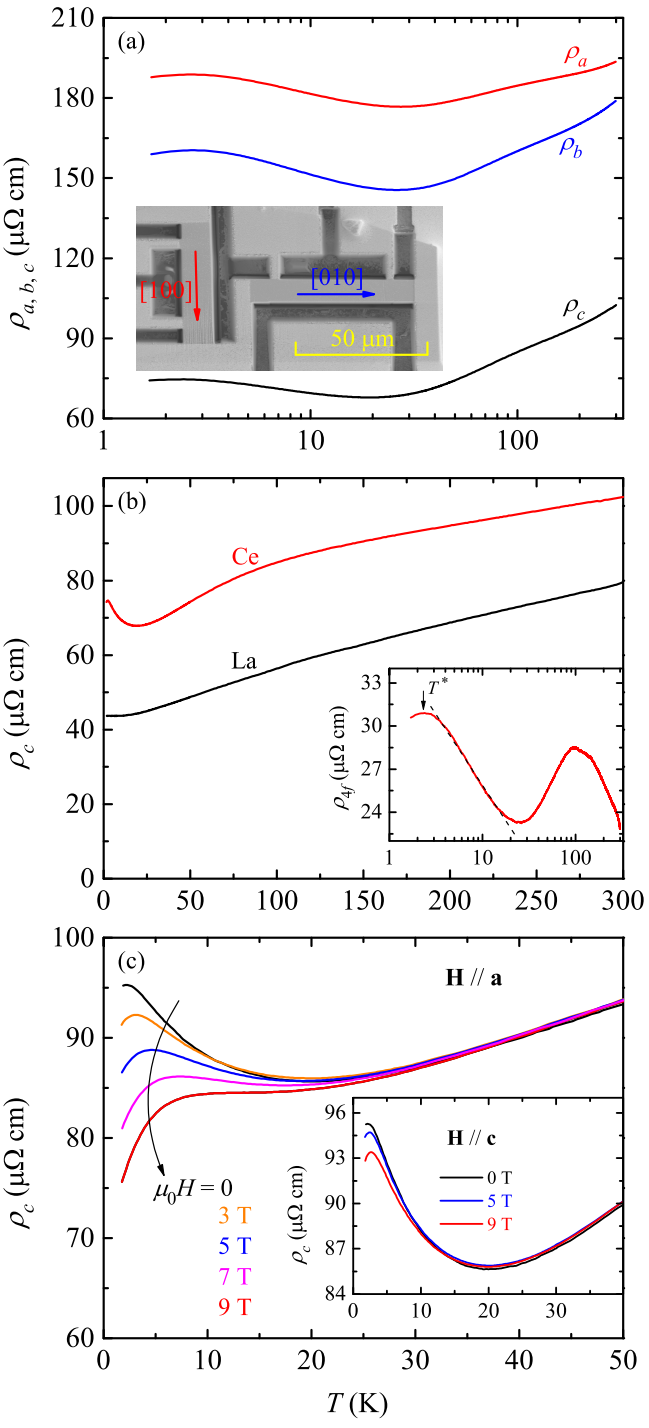

FIG. 2. (a) ρ_a, ρ_b, and ρ_c as functions of T for $Ce_2Rh_{3+\delta}Sb_4$. The inset shows the scanning-electron-microscope image of the microstructured device made by FIB to measure ρ_a and ρ_b. (b) Temperature-dependent ρ_c of $Ln_2Rh_{3+\delta}Sb_4$ [Ln = La (black) and Ce (red)]. The inset shows $\rho_{4f} \equiv \rho_c^{Ce} - \rho_c^{La}$. T^* signifies the temperature where ρ_{4f} starts to decrease. (c) $\rho_c(T)$ profiles at different magnetic fields **H** ∥ **a**. The inset shows the results for **H** ∥ **c**.

c direction, and these chains are well separated by Rh-Sb polyhedra. It is worthwhile to mention that viewing along **a**, the Ce atoms in each **bc** plane build up a distorted triangular network, and these networks are stacked along **a** following

TABLE I. Single-crystal XRD refinement data for $Ce_2Rh_{3+\delta}Sb_4$ at 290 K.

composition	$Ce_2Rh_{3.123}Sb_4$
formula weight (g/mol)	1088.32
space group	*Pnma* (No. 62)
a (Å)	16.1927(11)
b (Å)	10.9917(8)
c (Å)	4.5613(3)
V (Å^3)	811.84(10)
Z	4
ρ (g/cm^3)	8.904
2θ range	4.478–53.996°
no. of reflections, R_{int}	9097, 0.0749
no. of independent reflections	959
no. of parameters	62
R_1 [a], wR_2 [b], $[I > 2\delta(I)]$	0.0282, 0.0578
R_1, wR_2 (all data)	0.0307, 0.0587
goodness of fit on F^2	1.108
largest diffraction peak and hole (e/Å^3)	2.02 and −1.90

[a] $R_1 = \sum ||F_{obs}| - |F_{cal}|| / \sum |F_{obs}|$.
[b] $wR_2 = [\sum w(F_{obs}^2 - F_{cal}^2)^2 / \sum w(F_{obs}^2)^2]^{1/2}$, $w = 1/[\sigma^2 F_{obs}^2 + (aP)^2 + bP]$, where $P = [\max(F_{obs}^2) + 2F_{cal}^2]/3$.

the sequence of Ce2-Ce1′-Ce2-Ce1-Ce2; see Fig. 1(b). Such a triangular sublattice is speculated to cause some frustration effect to Ce magnetism, and it will be further discussed later on. The local environments of Ce1 and Ce2 are depicted in Fig. 1(c). More details about the crystalline structure of $Ce_2Rh_{3+\delta}Sb_4$ can be found in Tables I and II.

Temperature-dependent resistivity of $Ce_2Rh_{3+\delta}Sb_4$ for electrical current parallel to different principal axes is shown in Fig. 2(a). The base temperature of our resistivity measurements was 1.7 K. The profiles of $\rho_{a,b,c}(T)$ look similar except for their different magnitudes, $\rho_a > \rho_b > \rho_c$, following the same sequence of a, b, and c lengths. We should also point out that the interchain resistivity $\rho_{a,b}$ is about two times that of the intrachain ρ_c, characteristic of the quasi-1D electronic property. At low temperature below ∼25 K, a $-\log T$ dependence can be observed in all $\rho_{a,b,c}(T)$, which is commonly associated with the incoherent Kondo effect in heavy-fermion materials.

To better understand the electronic correlation effect in $Ce_2Rh_{3+\delta}Sb_4$, we now focus on ρ_c; for comparison, the results of $La_2Rh_{3+\delta}Sb_4$ are also displayed; see Fig. 2(b). While $La_2Rh_{3+\delta}Sb_4$ behaves like a conventional metal, the $\rho_c(T)$ of $Ce_2Rh_{3+\delta}Sb_4$ shows rather different features. Upon cooling, $\rho_c(T)$ decreases linearly until ∼100 K, where its slope gradually increases. Below ∼25 K, ρ_c turns up again. To get a clear insight into the scattering rate due to the $4f$ electrons, we calculate ρ_{4f} by subtracting ρ_c^{La} from ρ_c^{Ce}, as shown in the inset to Fig. 1(b). The bump centered around 100 K can now be clearly seen in ρ_{4f}. We attribute this to spin scatterings caused by the excitations between crystalline electric field (CEF) levels, and this can be further supported by specific-heat measurements (see below). Incoherent Kondo scattering sets in below 25 K, as evidenced by the logarithmic T-dependent ρ_{4f}. At low temperature, ρ_{4f} maximizes at $T^* = 2.4$ K, below which it falls back. At first glance, such a peak in $\rho_{4f}(T)$ might be

TABLE II. Structural parameters and equivalent isotropic displacement parameters U_{eq} of $Ce_2Rh_{3+\delta}Sb_4$. U_{eq} is taken as 1/3 of the trace of the orthogonalized U_{ij} tensor.

Atoms	Wyck.	x	y	z	Occ.	U_{eq}(Å^2)
Ce1	4c	0.25047(4)	0.91519(6)	0.2500	1.000	0.00609(17)
Ce2	4c	0.50390(4)	0.74876(6)	0.2500	1.000	0.00874(17)
Sb1	4c	0.43235(4)	0.05274(6)	0.2500	1.000	0.00581(19)
Sb2	4c	0.65227(4)	0.27291(6)	0.2500	1.000	0.00750(19)
Sb3	4c	0.29111(5)	0.11744(7)	0.7500	1.000	0.0079(2)
Sb4	4c	0.39686(5)	0.43626(7)	0.2500	1.000	0.00861(19)
Rh1	4c	0.55703(5)	0.46494(8)	0.2500	1.000	0.0052(2)
Rh2	4c	0.59242(5)	0.05378(8)	0.2500	1.000	0.0065(2)
Rh3	4c	0.31887(5)	0.22375(8)	0.2500	1.000	0.0070(2)
Rh4	4c	0.3485(7)	0.6227(9)	0.2500	0.123(3)	0.029(2)

reminiscent of the onset of Kondo coherence. However, we notice that this peak is strongly field-dependent; see Fig. 2(c). This is especially so when magnetic field is applied within the easy plane, viz., the peak at T^* moves upwards rapidly and meanwhile its height is also suppressed drastically. Such a significant field dependence is far beyond a regular field effect on coherent Kondo scattering [29], but it is more attributable to a field-induced polarization that reduces spin-flip scattering [30,31]. In this sense, magnetic ordering or at least short-range magnetic correlation would be likely at lower temperature. To clarify this issue, we turn to magnetic susceptibility measurements.

Figure 3(a) shows the temperature dependence of magnetic susceptibility ($\chi \equiv M/H$) of $Ce_2Rh_{3+\delta}Sb_4$, measured for different field orientations. One clearly sees that χ_a and χ_b are much larger than χ_c, confirming **ab** as the easy plane. The powder-averaged magnetic susceptibility is calculated via $\chi_{avg} = (\chi_a + \chi_b + \chi_c)/3$. For temperature above 100 K, $\chi_{avg}(T)$ obeys the standard Curie-Weiss formula, $\chi_{avg}(T) = C_0/(T - \theta_W)$, where C_0 is the Curie constant and θ_W is the Weiss temperature (note that the temperature-independent term χ_0 turns out to be negligibly small here). The fitting yields $\theta_W = -27.5$ K and the effective moment $\mu_{eff} = 2.56\mu_B$, very close to that of a free Ce^{3+} ion, $2.54\mu_B$. This implies that the $4f$ electron is highly localized and Rh ions are essentially nonmagnetic. The derived negative θ_W suggests antiferromagnetic correlation dominant in $Ce_2Rh_{3+\delta}Sb_4$. Indeed, χ_a, χ_b, and χ_c all show a clear peak near $T_N = 1.4$ K, characteristic of AFM transition.

The AFM ordering in $Ce_2Rh_{3+\delta}Sb_4$ is further supported by isothermal field-dependent magnetization [$M(H)$] shown in Fig. 3(b). At 0.42 K, well below T_N, M_c increases linearly with H and it reaches $0.3\mu_B$/Ce at 7 T, whereas M_a and M_b grow rapidly with H and tend to saturate at 1.4 and $1.1\mu_B$/Ce, respectively. Such anisotropy reaffirms that **c** is the hard axis, and the Ce moments are aligned within the **ab** plane. Another important feature in $M(H)$ is that the slope maximizes at 1.7 and 1.2 T for M_a and M_b, respectively, which may correspond to field-induced metamagnetic transitions. This provides additional evidence for the AFM ground state in $Ce_2Rh_{3+\delta}Sb_4$.

In Fig. 4(a), we present the temperature-dependent specific heat (C) of $Ce_2Rh_{3+\delta}Sb_4$. For comparison, $C(T)$ of the non-f reference $La_2Rh_{3+\delta}Sb_4$ is also shown. At high

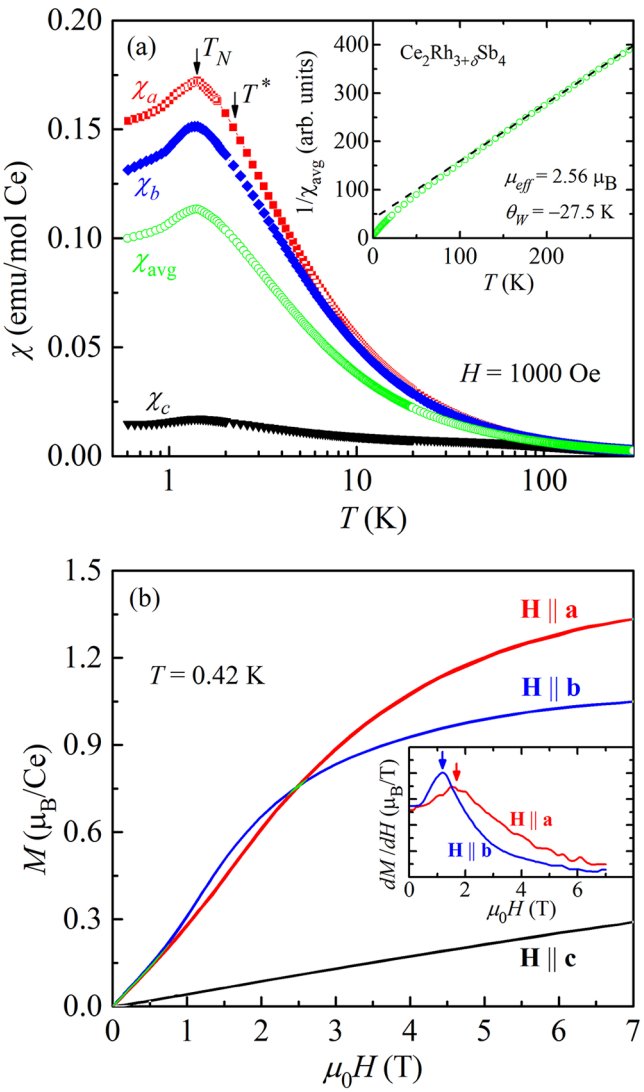

FIG. 3. (a) Temperature dependence of the magnetic susceptibility χ at 0.1 T measured with different field orientations. The inset shows $1/\chi_{avg}$ as a function of T, where χ_{avg} is the powder-averaged magnetic susceptibility. The dashed line stands for Curie-Weiss fitting. (b) Isothermal field-dependent magnetization at 0.42 K. The inset of (b), dM/dH curves. The red and blue arrows mark the metamagnetic transitions observed in M_a and M_b, respectively.

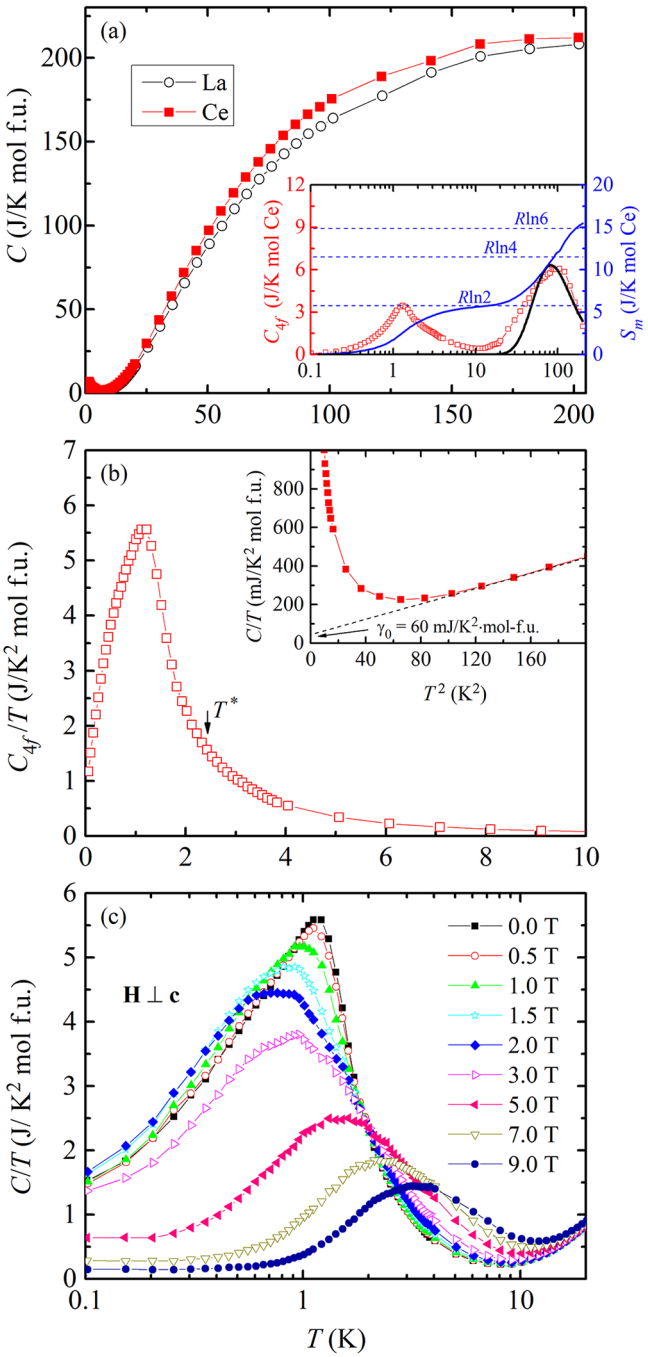

FIG. 4. (a) Temperature-dependent specific heat of $Ce_2Rh_{3+\delta}Sb_4$ and $La_2Rh_{3+\delta}Sb_4$. The inset shows the specific heat from $4f$ electrons and magnetic entropy (per molar Ce) as functions of T. The black solid line is a three-doublet Schottky anomaly fitting with $\Delta_1 = 210$ K and $\Delta_2 = 227$ K. (b) C_{4f}/T vs T. Note that the nuclear quadrupolar Schottky contribution that appears below 0.3 K has already been removed by properly fitting to a $1/T^3$ law [32]. The inset plots C/T vs T^2, which yields $\gamma_0 = 60$ mJ/K^2 mol f.u. (c) Temperature dependence of C/T measured at various magnetic fields $\mathbf{H} \perp \mathbf{c}$.

temperature, $C(T)$ tends to saturate to the classic limit $3NR = 224.5$ J/K mol f.u. given by Dulong-Petit's law [33], where $R = 8.314$ J/K mol is the ideal gas constant, and $N = 9$ is the number of atoms in a formula unit of stoichiometric $Ce_2Rh_3Sb_4$. A peak can be seen in $C(T)$ at around 1.4 K, which should be a consequence of the magnetic phase transition as observed in magnetic susceptibility. The normal-state Sommerfeld coefficient can be derived by linearly extrapolating C/T versus T^2 in the paramagnetic regime to zero, $\gamma_0 = 60$ mJ/K^2 mol f.u. [cf. the inset to Fig. 4(b)], a value moderately enhanced by a factor of 3 as compared to that of $La_2Rh_{3+\delta}Sb_4$ [25]. Such an enhancement should arise from the $4f$ electronic correlation effect. The contribution from $4f$ electrons, C_{4f}, is derived by subtracting the specific heat of $La_2Rh_{3+\delta}Sb_4$, and the result is displayed in the inset to Fig. 4(a). A broad peak centered at ~100 K is clearly visible, which should be a consequence of Schottky anomaly due to CEF splitting of a Ce^{3+} multiplet ($J = 5/2$).

The low-temperature AFM transition is now clearly seen in C_{4f}/T as shown in the main frame of Fig. 4(b). It should be pointed out that this peak does not appear λ-shaped, but is rather symmetric and has a long tail at the right-hand side, suggesting the presence of short-range ordering above T_N, and this is in agreement with the features of $\rho_c(T)$ and $\chi(T)$.

We then investigate the magnetic entropy S_m (per molar cerium) by integrating C_{4f}/T over T, as shown in the inset to Fig. 4(a). The entropy gain reaches $0.49R \ln 2$ and $0.73R \ln 2$ at T_N and T^*, respectively, manifesting a Kramers doublet ground state of Ce^{3+} in CEF. S_m gets fully recovered $R \ln 2$ near 10 K. The Kondo scale (T_K) can be estimated from $S_m(T_K/2) = 0.4R \ln 2$ [34]. This analysis yields $T_K \sim 2.4$ K, which is nearly the same as T^*. Therefore, $Ce_2Rh_{3+\delta}Sb_4$ represents a Kondo-lattice compound whose Kondo scale is comparable to the magnetic exchange, and furthermore, short-range ordering has played an important role in the reduced entropy gain at T_N. S_m approaches $R \ln 6$ at around 200 K, manifesting that the system has gradually recovered the full sextet degeneracy of Ce^{3+}. This is demonstrated by a three-doublet Schottky anomaly fitting with $\Delta_1 = 210$ K and $\Delta_2 = 227$ K, where Δ_i ($i = 1, 2$) are the energy difference between the ground and the ith excited doublet.

We also notice a salient feature that C_{4f}/T remains as large as ~1.2 J/K^2 mol f.u. even at the ultralow temperature 0.05 K. Such a large residual specific-heat coefficient is rather unusual for a long-range ordered antiferromagnet. In addition, a slope change is seen near 0.6 K in C_{4f}/T [Fig. 4(b)]. A naive thought is that a spin-reorientation takes place gradually within the AFM state. However, considering the two inequivalent Ce sites in the crystal structure, an alternative possibility could be that one set of the two Ce sublattices gives rise to the AFM transition at T_N, while the other Ce sublattice remains disordered (or becomes ordered at a lower temperature). This gives a reasonable explanation to the large residual specific-heat coefficient at $T \to 0$, as well as the slope change in C_{4f}/T.

In fact, the two inequivalent Ce sublattices can also be reflected in specific heat under a magnetic field ($\mathbf{H} \perp \mathbf{c}$), as shown in Fig. 4(c). On the whole, for a small applied field, the specific-heat peak near T_N is suppressed, consistent with the nature of AFM transition; upon further increasing the field, the peak gets broader and shifts to higher temperatures. Such an evolution is a consequence of the Schottky anomaly due to the reopening of the magnon gap caused by Zeeman splitting. This reflects a field-induced ferromagnetic ordering by

undergoing a metamagnetic transition, and it is in agreement with $\rho_c(T, H)$ and $M(H)$ mentioned earlier. Meanwhile, we notice that a shoulder appears in the C/T curve, which is most obviously seen at 2.0 and 3.0 T [Fig. 4(c)]. The appearance of this shoulder is probably due to the response to the external field from the originally disordered Ce sublattice. For larger fields, this shoulder gradually merges into the main peak and is no longer resolved, because both Ce sublattices are getting polarized. However, we must admit that to get a precise view of the magnetic structure, experiments like neutron scattering are required.

Finally, several additional remarks are in order:

(i) The origin of the low T_N. There could be multiple reasons for the low T_N in $Ce_2Rh_{3+\delta}Sb_4$. First, within a single Ce sublattice, the Ce-Ce distances are 4.56 and 5.95 Å [Fig. 1(b)], both of which are much larger than the typical values (3.8–4.2 Å) in most Ce-based intermetallic compounds [35]. The large Ce-Ce distance weakens the magnetic exchange severely. Note that the Ruderman-Kittel-Kasuya-Yosida (RKKY) exchange coupling decays rapidly with the intersite distance (r_{ij}) following $J_{\mathrm{RKKY}} \propto \frac{x\cos x - \sin x}{x^4}$, where $x = 2k_F r_{ij}$, and k_F is a Fermi wave vector [36]. The same scenario was also adopted for the low ordering temperature in $Ce_3Pt_{23}Si_{11}$ [37], $CeTm_2Cd_{20}$ (Tm = Co,Ni) [38], and $CeIr_3Ge_7$ [35]. In addition, since each Ce sublattice forms a distorted triangular network as displayed in Fig. 1(b), geometric frustration will probably reduce the ordering temperature further. The low T_N in $Ce_2Rh_{3+\delta}Sb_4$, as well as the comparable magnetic correlation and Kondo scales, makes it a novel candidate for further investigating quantum criticality under pressure.

(ii) The two inequivalent Ce sites. Although Ce1- and Ce2-sublattices build up the same distorted triangular networks [cf. Fig. 1(b)], their local environments are different. As shown in Fig. 1(c), both Ce1 and Ce2 are surrounded by 9 Rh (including Rh4) and 9 Sb sites, but Ce1 has three Rh4 neighbors, while Ce2 only has one. It is reasonable to infer that there are more conduction electrons around Ce2, and correspondingly, the extent of Kondo screening should also be stronger at Ce2. In this sense, strictly speaking, one would expect two different Kondo scales in this compound. It is interesting that multiple Ce-sites with different strengths of Kondo coupling and correspondingly distinct ground states have also been observed in $Ce_2Rh_3Sn_5$ [39] and $Ce_3Rh_4Sn_7$ [40].

IV. CONCLUSIONS

To summarize, using a Bi-flux method, we successfully synthesized single-crystalline $Ce_2Rh_{3+\delta}Sb_4$, a new dense Kondo lattice material. The compound contains quasi-1D Ce chains along **c**, which is also the magnetic hard axis. Quasi-1D electronic and magnetic features are unveiled by resistivity and magnetic susceptibility measurements. A long-range antiferromagnetic transition occurs at $T_N = 1.4$ K, while clear short-range ordering can be detected well above T_N. We attribute the low ordering temperature to the large Ce-Ce distance as well as the geometric frustration. Kondo scale is estimated to be about 2.4 K, comparable to the strength of magnetic exchange. Our work provides a rare paradigm of a dense Kondo lattice whose RKKY exchange and Kondo coupling are both weak but competing.

ACKNOWLEDGMENTS

The authors acknowledge Joe D. Thompson and Jinke Bao for helpful discussions. This work is supported by National Key R&D Program of China (2022YFA1602602 and 2022YFA1402200), the open research fund of Songshan Lake Materials Laboratory (2022SLABFN27), National Natural Science Foundation of China (11974306 and 12034017), Guangdong Basic and Applied Basic Research Foundation (2022B1515120020), and Key R&D Program of Zhejiang Province, China (2021C01002).

[1] G. R. Stewart, Rev. Mod. Phys. **73**, 797 (2001).
[2] P. W. Phillips, N. E. Hussey, and P. Abbamonte, Science **377**, eabh4273 (2022).
[3] M. Brando, D. Belitz, F. M. Grosche, and T. R. Kirkpatrick, Rev. Mod. Phys. **88**, 025006 (2016).
[4] C. Pfleiderer, G. J. McMullan, S. R. Julian, and G. G. Lonzarich, Phys. Rev. B **55**, 8330 (1997).
[5] S. Süllow, M. C. Aronson, B. D. Rainford, and P. Haen, Phys. Rev. Lett. **82**, 2963 (1999).
[6] Y. Luo, Y. Li, S. Jiang, J. Dai, G. Cao, and Z.-A. Xu, Phys. Rev. B **81**, 134422 (2010).
[7] A. Jesche, T. Ballé, K. Kliemt, C. Geibel, M. Brando, and C. Krellner, Phys. Status Solidi B **254**, 1600169 (2017).
[8] T. Westerkamp, M. Deppe, R. Küchler, M. Brando, C. Geibel, P. Gegenwart, A. P. Pikul, and F. Steglich, Phys. Rev. Lett. **102**, 206404 (2009).
[9] S. Lausberg, J. Spehling, A. Steppke, A. Jesche, H. Luetkens, A. Amato, C. Baines, C. Krellner, M. Brando, C. Geibel, H.-H. Klauss, and F. Steglich, Phys. Rev. Lett. **109**, 216402 (2012).
[10] C. Krellner, S. Lausberg, A. Steppke, M. Brando, L. Pedrero, H. Pfau, S. Tencé, H. Rosner, F. Steglich, and C. Geibel, New J. Phys. **13**, 103014 (2011).
[11] A. Steppke, R. Küchler, S. Lausberg, E. Lengyel, L. Steinke, R. Borth, T. Lühmann, C. Krellner, M. Nicklas, C. Geibel, F. Steglich, and M. Brando, Science **339**, 933 (2013).
[12] B. Shen, Y. Zhang, Y. Komijani, M. Nicklas, R. Borth, A. Wang, Y. Chen, Z. N. R. Li, X. Lu, H. Lee, M. Smidman, F. Steglich, P. Coleman, and H. Yuan, Nature (London) **579**, 51 (2020).
[13] D. Voßwinkel, O. Niehaus, U. C. Rodewald, and R. Pöttgen, Z. Naturforsch. B **67**, 1241 (2012).
[14] E. Matsuoka, C. Hondo, T. Fujii, A. Oshima, H. Sugawara, T. Sakurai, H. Ohta, F. Kneidinger, L. Salamakha, H. Michor, and E. Bauer, J. Phys. Soc. Jpn. **84**, 073704 (2015).
[15] P. Coleman and A. H. Nevidomskyy, J. Low Temp. Phys. **161**, 182 (2010).
[16] J. Custers, P. Gegenwart, H. Wilhelm, K. Neumaier, Y. Tokiwa, O. Trovarelli, C. Geibel, F. Steglich, C. Pepin, and P. Coleman, Nature (London) **424**, 524 (2003).

[17] A. Schröder, G. Aeppli, R. Coldea, M. Adams, O. Stockert, H. v. Löhneysen, E. Bucher, R. Ramazashvili, and P. Coleman, Nature (London) **407**, 351 (2000).
[18] S. Paschen, T. Lühmann, S. Wirth, P. Gegenwart, O. Trovarelli, C. Geibel, F. Steglich, P. Coleman, and Q. Si, Nature (London) **432**, 881 (2004).
[19] H. Shishido, R. Settai, H. Harima, and Y. Ōnuki, J. Phys. Soc. Jpn. **74**, 1103 (2005).
[20] Y. Luo, L. Pourovskii, S. E. Rowley, Y. Li, C. Feng, A. Georges, J. Dai, G. Cao, Z. Xu, Q. Si, and N. P. Ong, Nat. Mater. **13**, 777 (2014).
[21] Y. Komijani and P. Coleman, Phys. Rev. Lett. **120**, 157206 (2018).
[22] S. J. Yamamoto and Q. Si, Proc. Natl. Acad. Sci. (USA) **107**, 15704 (2010).
[23] T. R. Kirkpatrick and D. Belitz, Phys. Rev. Lett. **124**, 147201 (2020).
[24] J. Wang and Y.-F. Yang, Sci. China Phys. Mech. Astron. **65**, 257211 (2022).
[25] K. Cheng, W. Xie, S. Zou, H. Bu, J.-K. Bao, Z. Zhu, H. Guo, C. Cao, and Y. Luo, Mater. Futures **1**, 045201 (2022).
[26] R. Cardoso-Gil, N. Caroca-Canales, S. Budnyk, and W. Schnelle, Z. Kristallogr. **226**, 657 (2011).
[27] K. Schäfer, W. Hermes, U. C. Rodewald, R.-D. Hoffmann, and R. Pöttgen, Z. Naturforsch. **66**, 777 (2011).
[28] In this work, we have exchanged the **b** and **c** axes as compared with those in Ref. [25].
[29] A. D. Christianson, A. H. Lacerda, M. F. Hundley, P. G. Pagliuso, and J. L. Sarrao, Phys. Rev. B **66**, 054410 (2002).
[30] C. Krellner, N. S. Kini, E. M. Brüning, K. Koch, H. Rosner, M. Nicklas, M. Baenitz, and C. Geibel, Phys. Rev. B **76**, 104418 (2007).
[31] Y. Luo, J. Bao, C. Shen, J. Han, X. Yang, C. Lv, Y. Li, W. Jiao, B. Si, C. Feng, J. Dai, G. Cao, and Z.-a. Xu, Phys. Rev. B **86**, 245130 (2012).
[32] E. S. R. Gopal, *Specific Heats at Low Temperatures* (Plenum, New York, 1966).
[33] N. W. Ashcroft and N. D. Mermin, *Solid State Physics* (Saunders College, Philadelphia, 1976).
[34] P. Gegenwart, Q. Si, and F. Steglich, Nat. Phys. **4**, 186 (2008).
[35] B. K. Rai, J. Banda, M. Stavinoha, R. Borth, D.-J. Jang, K. A. Benavides, D. A. Sokolov, J. Y. Chan, M. Nicklas, M. Brando, C.-L. Huang, and E. Morosan, Phys. Rev. B **98**, 195119 (2018).
[36] M. A. Ruderman and C. Kittel, Phys. Rev. **96**, 99 (1954).
[37] C. Opagiste, C. Paulsen, E. Lhotel, P. Rodière, R.-M. Galera, P. Bordet, and P. Lejay, J. Magn. Magn. Mater. **321**, 613 (2009).
[38] B. D. White, D. Yazici, P.-C. Ho, N. Kanchanavatee, N. Pouse, Y. Fang, A. J. Breindel, A. J. Friedman, and M. B. Maple, J. Phys.: Condens. Matter **27**, 315602 (2015).
[39] M. B. Gamża, R. Gumeniuk, U. Burkhardt, W. Schnelle, H. Rosner, A. Leithe-Jasper, and A. Ślebarski, Phys. Rev. B **95**, 165142 (2017).
[40] P. Opletal, E. Duverger-Nédellec, K. Miliyanchuk, S. Malick, Z. Hossain, and J. Custers, J. Alloys Compd. **927**, 166941 (2022).